Fano interference in supported gold nanosandwiches with weakly coupled nanodisks

A. Mendoza-Galván,[1,*] K. Järrendahl,[2] A. Dmitriev,[3] T. Pakizeh,[4] M. Käll,[3] and H. Arwin[2,5]

[1]*Cinvestav-IPN, Unidad Querétaro, Libramiento Norponiente 2000, 76230 Querétaro, Mexico*
[2]*Laboratory of Applied Optics, Department of Physics, Chemistry and Biology, Linköping University, SE-581 83 Linköping, Sweden*
[3]*Department of Applied Physics, Chalmers University of Technology, SE-412 96 Göteborg, Sweden*
[4]*Faculty of Electrical and Computer Engineering, K. N. Toosi University of Technology, Tehran 16314, Iran*
[5]*hansa@ifm.liu.se*
[*]*amendoza@qro.cinvestav.mx*

Abstract: We studied the far-field optical response of supported gold-silica-gold nanosandwiches using spectroscopic ellipsometry, reflectance and transmittance measurements. Although transmittance data clearly shows that the gold nanodisks in the sandwich structure interact very weakly, oblique reflectance spectra of s- and p-polarized light show clearly asymmetric line-shapes of the Fano type. However, all experimental results are very well described by modeling the gold nanodisks as oblate spheroids and by employing a 2 × 2 scattering matrix formulation of the Fresnel coefficients provided by an island film theory. In particular, the Fano asymmetry can be explained in terms of interference between the scattered waves from the decoupled nanodisks in the spectral range limited by their respective plasmon resonances. We also show that the reflectance and ellipsometry spectra can be described by a three-layer system with uniaxial effective dielectric functions.

OCIS codes: (240.6680) Surface plasmons; (160.1190) Anisotropic optical materials; (160.1245) Artificially engineered materials; (260.2130) Ellipsometry and polarimetry; (160.4760) Optical properties.

References and links

1. N. J. Halas, S. Lal, W. S. Chang, S. Link, and P. Nordlander, "Plasmons in strongly coupled metallic nanostructures," Chem. Rev. **111**(6), 3913–3961 (2011).
2. V. M. Shalaev, W. Cai, U. K. Chettiar, H.-K. Yuan, A. K. Sarychev, V. P. Drachev, and A. V. Kildishev, "Negative index of refraction in optical metamaterials," Opt. Lett. **30**(24), 3356–3358 (2005).
3. H.-K. Yuan, U. K. Chettiar, W. Cai, A. V. Kildishev, A. Boltasseva, V. P. Drachev, and V. M. Shalaev, "A negative permeability material at red light," Opt. Express **15**(3), 1076–1083 (2007).
4. E. Pshenay-Severin, A. Chipouline, J. Petschulat, U. Hübner, A. Thünnerman, and T. Pertsch, "Optical properties of metamaterials based on asymmetric double-wire structures," Opt. Express **19**(7), 6269–6283 (2011).
5. A. Christ, Y. Ekinci, H. H. Solak, N. A. Gippius, S. G. Tikhodeev, and O. J. F. Martin, "Controlling the Fano interference in a plasmonic lattice," Phys. Rev. B **76**(20), 201405 (2007).
6. A. Christ, O. J. F. Martin, Y. Ekinci, N. A. Gippius, and S. G. Tikhodeev, "Symmetry breaking in a plasmonic metamaterial at optical wavelength," Nano Lett. **8**(8), 2171–2175 (2008).
7. Y. Ekinci, A. Christ, M. Agio, O. J. F. Martin, H. H. Solak, and J. F. Löffler, "Electric and magnetic resonances in arrays of coupled gold nanoparticle in-tandem pairs," Opt. Express **16**(17), 13287–13295 (2008).
8. Y. Jeyaram, S. K. Jha, M. Agio, J. F. Löffler, and Y. Ekinci, "Magnetic metamaterials in the blue range using aluminum nanostructures," Opt. Lett. **35**(10), 1656–1658 (2010).
9. Q. Li and G. P. Wang, "Tunable photonic metamaterials in the near infrared frequencies," Opt. Express **18**(13), 14123–14128 (2010).
10. A. Dmitriev, T. Pakizeh, M. Käll, and D. S. Sutherland, "Gold-silica-gold nanosandwiches: tunable bimodal plasmonic resonators," Small **3**(2), 294–299 (2007).
11. T. Pakizeh, A. Dmitriev, M. S. Abrishamian, N. Granpayeh, and M. Käll, "Structural asymmetry and induced optical magnetism in plasmonic nanosandwiches," J. Opt. Soc. Am. B **25**(4), 659–667 (2008).
12. T. Pakizeh, M. S. Abrishamian, N. Granpayeh, A. Dmitriev, and M. Käll, "Magnetic-field enhancement in gold nanosandwiches," Opt. Express **14**(18), 8240–8246 (2006).

#178926 - $15.00 USD Received 1 Nov 2012; revised 28 Nov 2012; accepted 28 Nov 2012; published 20 Dec 2012

13. C. Tserkezis, N. Papanikolaou, G. Gantzounis, and N. Stefanou, "Understanding artificial optical magnetism of periodic metal-dielectric-metal layered structures," Phys. Rev. B **78**(16), 165114 (2008).
14. L. Qiu, S. Wang, H. Liu, T. Li, S. Zhu, and X. Zhang, "Magnetic plasmon in coupled nanosandwich structure," J. Opt. Soc. Am. B **28**(7), 1655–1660 (2011).
15. J. Parsons, E. Hendry, J. R. Sambles, and W. L. Barnes, "Localized surface-plasmon resonances and negative refractive index in nanostructured electromagnetic metamaterials," Phys. Rev. B **80**(24), 245117 (2009).
16. B. Gallinet and O. J. F. Martin, "Influence of electromagnetic interactions on the line shape of plasmonic Fano resonances," ACS Nano **5**(11), 8999–9008 (2011).
17. T. Pakizeh, C. Langhammer, I. Zorić, P. Apell, and M. Käll, "Intrinsic Fano interference of localized plasmons in Pd nanoparticles," Nano Lett. **9**(2), 882–886 (2009).
18. M. Svedendahl and M. Käll, "Fano interference between localized plasmons and interface reflections," ACS Nano **6**(8), 7533–7539 (2012).
19. A. E. Miroshnichenko, S. Flach, and Y. S. Kivshar, "Fano resonances in nanoscale structures," Rev. Mod. Phys. **82**(3), 2257–2298 (2010).
20. B. Luk'yanchuk, N. I. Zheludev, S. A. Maier, N. J. Halas, P. Nordlander, H. Giessen, and C. T. Chong, "The Fano resonance in plasmonic nanostructures and metamaterials," Nat. Mater. **9**(9), 707–715 (2010).
21. B. Gallinet and O. J. F. Martin, "Ab initio theory of Fano resonances in plasmonic nanostructures and metamaterials," Phys. Rev. B **83**(23), 235427 (2011).
22. N. A. Mirin, K. Bao, and P. Nordlander, "Fano resonances in plasmonic nanoparticle aggregates," J. Phys. Chem. A **113**(16), 4028–4034 (2009).
23. A. Pannipitiya, I. D. Rukhlenko, M. Premaratne, H. T. Hattori, and G. P. Agrawal, "Improved transmission model for metal-dielectric-metal plasmonic waveguides with stub structure," Opt. Express **18**(6), 6191–6204 (2010).
24. X. Piao, S. Yu, S. Koo, K. Lee, and N. Park, "Fano-type spectral asymmetry and its control for plasmonic metal-insulator-metal stub structures," Opt. Express **19**(11), 10907–10912 (2011).
25. H. Fredriksson, Y. Alaverdyan, A. Dmitriev, C. Langhammer, D. S. Sutherland, M. Zäch, and B. Kasemo, "Hole–mask colloidal lithography," Adv. Mater. (Deerfield Beach Fla.) **19**(23), 4297–4302 (2007).
26. K. L. Kelly, E. Coronado, L. L. Zhao, and G. C. Schatz, "The optical properties of metal nanoparticles: the influence of size, shape, and dielectric environment," J. Phys. Chem. B **107**(3), 668–677 (2003).
27. D. Bedeaux and J. Vlieger, *Optical Properties of Surfaces* (Imperial College Press, 2001).
28. T. Yamaguchi, S. Yoshida, and A. Kinbara, "Optical effect of the substrate on the anomalous absorption of aggregated silver films," Thin Solid Films **21**(1), 173–187 (1974).
29. K. Johansen, H. Arwin, I. Lundström, and B. Liedberg, "Imaging surface plasmon resonance sensor based on multiple wavelengths: Sensitivity considerations," Rev. Sci. Instrum. **71**(9), 3530–3538 (2000).
30. A. Mendoza-Galván, K. Järrendahl, A. Dmitriev, T. Pakizeh, M. Käll, and H. Arwin, "Optical response of supported gold nanodisks," Opt. Express **19**(13), 12093–12107 (2011).
31. V. A. Fedotov, V. I. Emel'yanov, K. F. MacDonald, and N. I. Zheludev, "Optical properties of closely packed nanoparticle films: spheroids and nanoshells," J. Opt. A, Pure Appl. Opt. **6**(2), 155–160 (2004).
32. H. Wormeester, E. S. Kooij, A. Mewe, S. Rekveld, and B. Poelsema, "Ellipsometric characterisation of heterogeneous 2D layers," Thin Solid Films **455–456**, 323–334 (2004).
33. R. M. A. Azzam and N. M. Bashara, *Ellipsometry and Polarized Light* (North Holland, , 1977).

1. Introduction

Metal-dielectric composite nanostructures support confined electron oscillations driven by electromagnetic waves, i.e. localized surface plasmon resonances. Bringing together two or more metal nanoparticles, the plasmon resonances interact and coupled resonances emerge [1], as has been shown for several stacked configurations comprised of strips [2,3], cut-wires [4–6], and nanodisks [7–11] supported on a substrate. Several of these metal-dielectric-metal nanostructures show symmetric and asymmetric coupled resonances, where the latter has been interpreted as producing optical magnetism. In particular, the optical response of nanostructures comprised by metallic nanodisks in-tandem pairs (nanosandwiches) has been subject of several experimental and theoretical reports [12–15]. Besides of optical magnetism in nanosandwiches, Fano resonances have been reported in their normal incidence reflectance spectra and has been explained by using numerical simulations [7,8]. The Fano resonance is characterized by an asymmetric line-shape that results from the interference between a broad continuum spectrally overlapped by a narrower resonance. The Fano resonance phenomenon is commonly found in diverse metallic nanostructures [5–8,16–18] and the subject has been reviewed recently [19,20].

Generally, the optical response of plasmonic nanostructures is analyzed by numerical methods, often at high computational costs, and analytical descriptions involving the influence of electromagnetic interactions on the resonance line shape are scarce [21–24]. Furthermore, most of the previous reports are based on measurements of transmittance and/or

#178926 - $15.00 USD Received 1 Nov 2012; revised 28 Nov 2012; accepted 28 Nov 2012; published 20 Dec 2012

reflectance at normal incidence. Owing to the intrinsic anisotropy of the nanostructures, such analysis is limited because only the in-plane component of the polarizability is probed. Therefore, appropriate modeling of optical measurements at oblique incidence is required to explain the observed phenomena identifying the individual contributions in composite nanostructures. Understanding the optical properties of weakly interacting nanodisks in a nanosandwich structure can serve as a first step in analysis of more complex anisotropic structures.

In this work, we investigate the optical response of gold-silica-gold nanosandwiches fabricated by hole-mask colloidal lithography, which produces short-range ordered structures covering large areas [25]. Spectroscopic ellipsometry and irradiance measurements at oblique and normal incidence are used to probe the in-plane as well as the out-of-plane components. Experimental evidence of weak coupling and interference effects are discussed in Sec. 3.1. The gold nanodisks in the sandwich structure are modeled as oblate spheroids in Sec. 3.2 and the polarizabilities in a modified long wavelength approximation [26] including interaction with the substrate are calculated. In Sec. 3.3 generalities of the island film theory [27] and the modified Fresnel coefficients in the Abelès 2×2 scattering matrix formalism are described. The latter formalism is applied in Sec. 3.4 to investigate interference effects and a comparison is made between model-calculated data and experimental spectra. Finally, in Sec. 3.5 the homogenization of the individual uniaxial layers is explored using effective dielectric functions of the Yamaguchi type [28].

2. Experimental

Arrays of gold-silica-gold nanosandwiches were fabricated on glass substrates by hole-mask colloidal lithography [25]. Details of thickness and diameter control during fabrication of nanosandwiches can be found elsewhere [10,11]. The fabrication process produces truncated cone-shaped structures schematically represented in the inset of Fig. 1. In the present work the bottom and top gold nanodisks have average diameters of 170 and 120 nm, respectively. The two gold nanodisks are 20 nm thick and the thickness of the silica spacer is 40 nm.

Spectroscopic ellipsometry (SE) measurements were performed in the 300-1300 nm wavelength range at angles of incidence between 40 and 70° using a variable angle spectroscopic ellipsometer (VASE) of rotating analyzer type equipped with an auto-retarder (J. A. Woollam Co., Inc.). Reflectance spectra were measured for polarizations parallel and perpendicular to the plane of incidence at angles of incidence ranging from 20 to 70°. For ellipsometry and reflectance measurements the back-side of the substrate was roughened. Also, transmittance (s-polarized) spectra at normal incidence and 25° angle of incidence were acquired. The refractive index of the glass substrate was determined from ellipsometric data and the extinction coefficient was subsequently obtained by a point-by-point fitting of transmittance spectra at normal incidence. The complex dielectric function of gold was taken from VASE measurements of a homogeneous gold film [29].

3. Results and discussion

3.1 Weakly coupled plasmon resonances

Figure 1(a) shows a comparison between transmittance (T) spectra measured at normal incidence, for the nanosandwich sample and a layer of 20 nm thick silica-capped gold nanodisks. We reported on the optical response of the latter sample in a previous work [30]. The structure and relevant parameters of the two samples are schematically represented in the insets of Fig. 1. It can be observed that the spectrum of the sandwiched structure consists of two plasmon resonances with nearly symmetric line-shapes; one weak resonance at 620 nm and a stronger mode at 810 nm. This result is in contrast to previously published results for nanosandwiches constructed from strongly coupled nanodisks. Such structures typically exhibit two hybridized resonances, that is, a strong high frequency mode and a weak low-frequency mode that correspond to the in-phase and anti-phase motion of the individual dipolar particle plasmons [7–11]. Furthermore, it is clear from Fig. 1(a) that the T spectra of

#178926 - $15.00 USD Received 1 Nov 2012; revised 28 Nov 2012; accepted 28 Nov 2012; published 20 Dec 2012

the nanosandwiches and of the 170 nm diameter nanodisks are essentially identical for wavelengths longer than ~700 nm. As shown in Fig. 1(b), the s-polarized (T_s) transmittance spectra at an angle of incidence of 25° are nearly identical to the ones taken at normal incidence, in particular, the symmetric line-shape of the nanosandwich spectrum is retained. The results demonstrate that the plasmon resonances of the composite nanosandwich structure are well approximated by the dipole modes of the individual 120 nm and 170 nm nanodisks and, consequently, that plasmon hybridization is weak. This result is expected when considering that the 40 nm vertical separation between the disks is considerably larger than the 20 nm thickness of the individual nanodisks in the sandwich, as well as by considering the large difference in nanodisk aspect ratio, leading to nondegenerate modes.

Figure 1(c) compares reflectance spectra for the two samples discussed above. Since reflection measurements at near normal incidence are not possible in the experimental setup used, we instead show s-polarized reflectance (R_s) spectra at an angle of incidence of 20°. In the case of nanosandwich spectrum, one clearly observes asymmetric Fano-like line-shapes, in particular for the short-wavelength mode. A similar asymmetric line-shape was found for p-polarized reflectance (not shown). Notice that the maximum of R_s in Fig. 1(c) at 810 nm is almost identical to that of the silica-capped gold nanodisks, similar to the case of transmittance in Figs. 1(a) and 1(b).

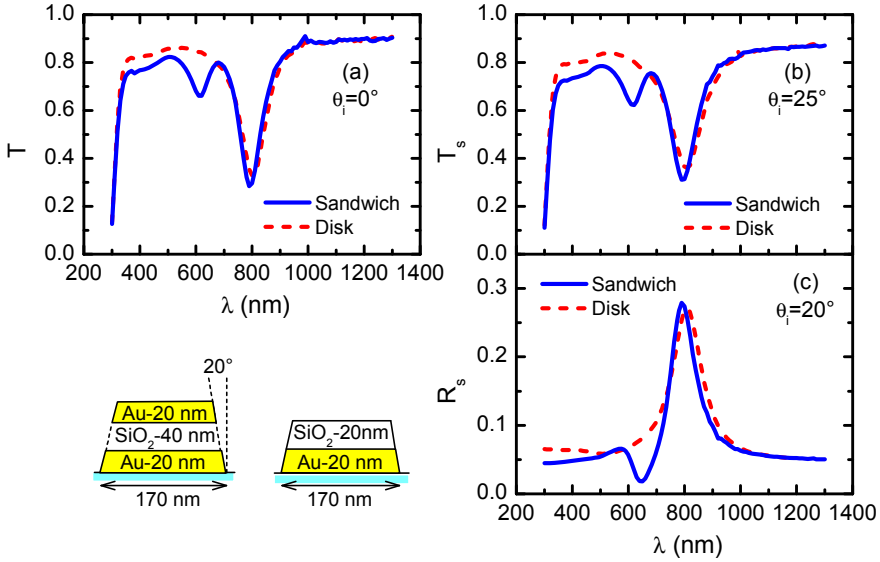

Fig. 1. Experimental spectra of nanosandwiches and silica-capped nanodisks: (a) normal incidence transmittance; (b) s-polarized transmittance at angle of incidence of 25°; s-polarized reflectance at angle of incidence of 20°. The insets schematically show the nanosandwich (left) and nanodisk (right) structures.

3.2 Nanodisk polarizabilities

According to the interpretation of the transmission spectra in Fig. 1, it is instructive to analyze the individual optical response of the decoupled nanodisks in the sandwiched structure. For that, and as in our previous work [30], the nanodisks are modeled as oblate spheroids with the major (minor) semi-axis a_j (c_j) parallel (perpendicular) to the substrate. The sub-index j = 1(2) identifies the nanodisk at the bottom (top) as shown in the insets of Figs. 2(b) and 2(c), in the latter s is the thickness of the silica spacer. Thus, the spheroids optical response is expressed in terms of two polarizabilities: one in-plane $\alpha_{j,\parallel}$ and one out-of-plane $\alpha_{j,\perp}$ which are given by [27,30],

#178926 - $15.00 USD Received 1 Nov 2012; revised 28 Nov 2012; accepted 28 Nov 2012; published 20 Dec 2012

$$\alpha_{j(\|,\perp)} = \frac{4\pi a_j^2 c_j}{3} \frac{\varepsilon_a (\varepsilon_m - \varepsilon_a)}{\left[\varepsilon_a + L_{j(\|,\perp)} (\varepsilon_m - \varepsilon_a)\right]}, \quad (1)$$

where ε_a and ε_m are the ambient and nanodisks dielectric functions, respectively. For the in-plane component, the effective depolarization factor in Eq. (1) is given by [30],

$$L_{j,\|} = l_{j,\|} - L_{j,sub} - \frac{k^2 a_j c_j}{3} - \frac{2ik^3 a_j^2 c_j}{9}, \quad (2)$$

where $l_{j,\|}$ is the depolarization factor in the electrostatic limit and $L_{j,sub}$ accounts for the interaction with the substrate using the spheroidal field [31], viz.,

$$l_{j,\|} = \frac{\eta_j^2}{2\left(\eta_j^2 - 1\right)^{3/2}} \left[\arctan\left(\sqrt{\eta_j^2 - 1}\right) - \frac{\sqrt{\eta_j^2 - 1}}{\eta_j^2} \right], \quad (3)$$

and,

$$L_{j,sub} = \varepsilon_a \frac{\varepsilon_a - \varepsilon_s}{\varepsilon_a + \varepsilon_s} \frac{\eta_j^2}{2\left(\eta_j^2 - 1\right)^{3/2}} \left[\frac{\left(d_j / c_j\right)\sqrt{\eta_j^2 - 1}}{\eta_j^2 + \left(d_j / c_j\right)^2 - 1} - \arctan\left(\frac{\sqrt{\eta_j^2 - 1}}{\left(d_j / c_j\right)} \right) \right], \quad (4)$$

where $\eta_j = a_j/c_j$ is the spheroid aspect ratio and d_j is the distance between the spheroid and its image in the substrate with dielectric function ε_s. The effective depolarization factor for the out-of-plane polarizability in Eq. (1) is $L_{j,\perp} = l_{j,\perp}\text{-}2L_{j,sub}$ where $l_{j,\perp} = 1\text{-}2l_{j,\|}$. The expressions of $l_{j,\|}$ and $L_{j,sub}$ in Eqs. (3) and (4) explicitly show their dependence on the spheroid aspect ratio $\eta_j = a_j/c_j$. The third and fourth terms of Eq. (2) correspond to dynamic depolarization and radiation damping [30], respectively, where $k = 2\pi/\lambda$ is the wave number of the incident light.

Figure 2 shows the nanodisks polarizabilities, $\alpha_{j,\|}$ and $\alpha_{j,\perp}$, calculated with Eqs. (1)-(4), using the nominal parameters of the nanosandwich structure: $a_1 = 85$ nm, $a_2 = 60$ nm, $c_1 = c_2 = 10$ nm, and $s = 40$ nm. It is clear from Fig. 2 that $\left|\alpha_{1,\|}\right| > \left|\alpha_{2,\|}\right|$ and $\left|\alpha_{1,\perp}\right| > \left|\alpha_{2,\perp}\right|$ which is mainly due to the larger volume of the bottom nanodisk. As was previously reported, the interaction with the substrate enhances (and shifts to longer wavelengths) the plasmon resonance of supported gold nanodisks [30]. In the present case, the distances d_j between the nanodisks and their respective images are $d_1 = 2c_1$ and $d_2 = 2(c_2 + s + 2c_1)$ for the bottom and top nanodisks, respectively. Since the interaction with the substrate decreases with d_j according to Eq. (4), $L_{1,sub} > L_{2,sub}$, implying a larger decrease of the effective depolarization factor $L_{1,\|}$ in Eq. (2) for the nanodisk at the bottom. The latter result and the dependence on $L_{1,\|}$ in Eq. (1) show how the interaction with the substrate contributes to the result $\left|\alpha_{1,\|}\right| > \left|\alpha_{2,\|}\right|$.

In the case of the out-of-plane polarizabilities, an important contribution to the result $\left|\alpha_{1,\perp}\right| > \left|\alpha_{2,\perp}\right|$ resides on the fact that the nanodisk at the bottom is sandwiched by the silica spacer and the substrate (inset of Fig. 1). Thus, for p-polarized incident light, screening charges are induced in these materials due to the normal component of the incident electric field. Therefore, for this component the surrounding ambient differs from air and in Eq. (1), ε_a was taken as that of fused silica in the calculation of the out-of-plane polarizability $\alpha_{1,\perp}$. It should be noted that the spectral position of the maxima in $\mathrm{Im}\{\alpha_{1,\|}\}$ and $\mathrm{Im}\{\alpha_{2,\|}\}$ at 810 and 620 nm, respectively, are coincident with the plasmon resonances in the T spectrum in Fig. 1(a). In Fig. 2(c), the steep rise of $\mathrm{Im}\{\alpha_{j,\perp}\}$ at wavelengths shorter than 500 nm can be attributed to the onset of interband transitions in gold. Furthermore, in Fig. 2(b) it is important to note that $\alpha_{1,\|}$ and $\alpha_{2,\|}$ differ in phase in the wavelength range between 620 and 810 nm.

#178926 - $15.00 USD Received 1 Nov 2012; revised 28 Nov 2012; accepted 28 Nov 2012; published 20 Dec 2012

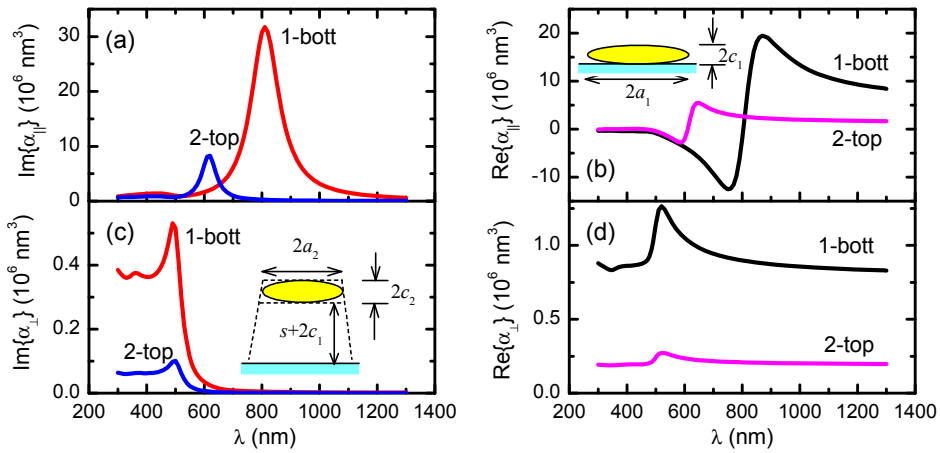

Fig. 2. Complex nanodisks polarizabilities: (a)-(b) in-plane $\alpha_{j,\parallel}$ and (c)-(d) out-of-plane $\alpha_{j,\perp}$. The insets in (b) and (c) schematically show the structural parameters for the nanodisks at the bottom and at the top, respectively.

3.3 Island film theory and 2 × 2 matrix Abelès formalism

The optical response of systems comprised by particles (islands) attached to a flat substrate has been successfully explained by the island film theory [27]. This theory is based on the concept of excess currents, charge densities and fields that modify the boundary conditions at the surface. For non-magnetic systems and in absence of spatial dispersion, the effect of those excess quantities is accounted for through constitutive relations in terms of two surface susceptibilities, one parallel (γ) and the other perpendicular (β) to the substrate. Thus, modified Fresnel coefficients are obtained, which for light polarized perpendicular r_s and parallel r_p to the plane of incidence are given by [27],

$$r_s = \frac{n_a \cos\theta_i - n_s \cos\theta_t + ik\gamma}{n_a \cos\theta_i + n_s \cos\theta_t - ik\gamma}, \tag{5}$$

and,

$$r_p = \frac{\kappa_- - ik\left[\gamma \cos\theta_i \cos\theta_t - n_a n_s \varepsilon_a \beta \sin^2\theta_i\right]}{\kappa_+ - ik\left[\gamma \cos\theta_i \cos\theta_t + n_a n_s \varepsilon_a \beta \sin^2\theta_i\right]}, \tag{6}$$

where,

$$\kappa_\pm = \left(n_s \cos\theta_i \pm n_a \cos\theta_t\right)\left[1 - k^2 \varepsilon_a \gamma\beta \sin^2\theta_i / 4\right]. \tag{7}$$

In Eqs. (5)-(7), n_a ($= \varepsilon_a^{1/2}$) and n_s ($= \varepsilon_s^{1/2}$) are the refractive indices of the ambient and substrate, respectively; θ_i and θ_t are the incidence and refraction angles, respectively, related by Snell's law $n_a \sin\theta_i = n_s \sin\theta_t$. The transmission coefficients for s- and p-polarization are given by [27],

$$t_s = 2n_a \cos\theta_i / D_s , \tag{8}$$

and,

$$t_p = 2n_a \cos\theta_i \left(1 + k^2 \gamma\beta\varepsilon_a \sin^2\theta_i / 4\right) / D_p , \tag{9}$$

where D_s and D_p are the denominators in Eq. (5) and (6), respectively.

#178926 - $15.00 USD Received 1 Nov 2012; revised 28 Nov 2012; accepted 28 Nov 2012; published 20 Dec 2012

In the case of non-interacting particles the constitutive coefficients are $\gamma = \rho\alpha_{\|}$ and $\beta = \rho\alpha_{\perp}/\varepsilon_a^2$, where ρ is the number of particles per unit area. Using this formalism, we previously studied the optical response of supported gold nanodisks approximated as oblate spheroids, Fig. 3(a) [30].

Because the composite structure of the nanosandwiches, it is necessary to consider the Abelès 2 × 2 matrix formalism of the island film theory which leads to the interface matrix [32],

$$\mathbf{I}_f = \frac{1}{t_f}\begin{bmatrix} 1 & -r_f \\ r_f & t_f^2 - r_f^2 \end{bmatrix}, \tag{10}$$

where r_f and t_f are the reflection and transmission coefficients of the hypothetical free-standing island film schematically represented in Fig. 3(b). Because the same medium is above and below the island film, the coefficients r_f and t_f for p- and s-polarizations in Eq. (10) are obtained from Eqs. (5)-(9) making $n_a = n_s$ and $\theta_i = \theta_t$, that is,

$$r_f^s = \frac{X_s}{1 - X_s}, \quad r_f^p = \frac{Z_p - Y_p}{\left(1 - Z_p\right)\left(1 - Y_p\right)}, \tag{11}$$

and,

$$t_f^s = \frac{1}{1 - X_s}, \quad t_f^p = \frac{1 - Y_p Z_p}{\left(1 - Z_p\right)\left(1 - Y_p\right)}, \tag{12}$$

where,

$$X_s = \frac{ik\gamma}{2n_a \cos\theta_i}, \quad Y_p = \frac{ik\gamma\cos\theta_i}{2n_a}, \quad Z_p = \frac{ik\beta n_a^3 \sin^2\theta_i}{2\cos\theta_i}. \tag{13}$$

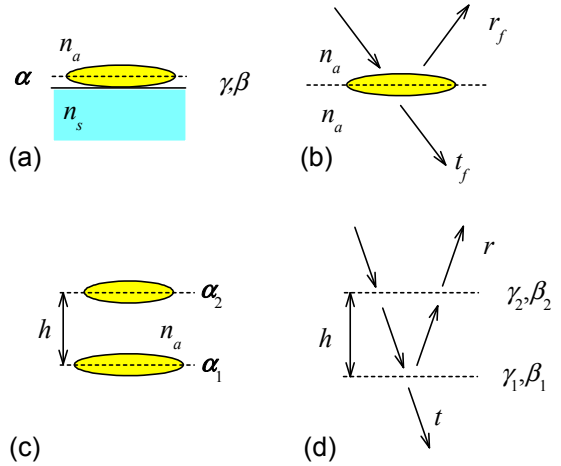

Fig. 3. Schematics of the analyzed systems: (a) supported oblate spheroids; (b) free-standing oblate spheroids; (c) two layers of free-standing oblate spheroids; (d) light propagation through two layers with different surface susceptibilities.

The 2 × 2 matrix formalism allows straightforward calculations of the optical response of stratified systems. In fact, Eqs. (5)-(9) follow from the ratios $r = S_{21}/S_{11}$ and $t = 1/S_{11}$ where S_{ij} are elements of the scattering matrix $\mathbf{S} = \mathbf{I}_f \mathbf{I}_{as}$ (for the corresponding polarization) being $\mathbf{I}_{as}$ the standard Abelès ambient-substrate interface matrix [33].

#178926 - $15.00 USD Received 1 Nov 2012; revised 28 Nov 2012; accepted 28 Nov 2012; published 20 Dec 2012

In the present work Eqs. (11)-(13) are of particular interest because they allow for an analysis of the individual optical response of the free-standing island layers, that is, with polarizabilities ($\alpha_{j,\parallel}$, $\alpha_{j,\perp}$) corresponding to the nanodisks at the bottom (j = 1) and at the top (j = 2) of the sandwich structure. For illustration purposes, we show in Fig. 4 only the normal incidence transmittance $T_j = \left|t_{f,j}\right|^2$ and oblique (θ_i = 50°) reflectance $R_j^{p,s} = \left|r_{f,j}^{p,s}\right|^2$ spectra of the surface susceptibilities $\gamma_j = \rho\alpha_{j,\parallel}$ and $\beta_j = \rho\alpha_{j,\perp}/\varepsilon_a^2$ with ρ = 4.5 μm^{-2}. Similar results were obtained for other angles of incidence. As expected, the T_j, R_j^{p} and R_j^{s} spectra peak at the corresponding spectral position of the maximum in Im$\{\alpha_{1,\parallel}\}$ or Im$\{\alpha_{2,\parallel}\}$ shown in Fig. 2(a). Nevertheless, the individual spectra of T_j, R_j^p, and R_i^s overlap to different extent in the range of 600 to 800 nm where the complex in-plane polarizabilities $\alpha_{j,\parallel} = \left|\alpha_{j,\parallel}\right|\exp\left(i\varphi_j\right)$ in Fig. 2 present the largest phase difference $\Delta\varphi = \varphi_1$-$\varphi_2$ as is shown in Fig. 4(d). Also, in Fig. 4(d) it is shown the spectral dependence of the phase difference of reflection coefficients $r_{f,j}^{p,s} = \left|r_{f,j}^{p,s}\right|\exp\left(i\varphi_j^{p,s}\right)$ in Eq. (10), for p- and s-polarization ($\Delta\varphi^{p,s} = \varphi_1^{p,s} - \varphi_2^{p,s}$) calculated at an angle of incidence of 50°. Clearly, the phase differences show similar wavelength dependences. Results similar to those in Fig. 4(d) were obtained also for reflection spectra calculated for other angles of incidence but such large phase differences were not found for the transmission coefficients.

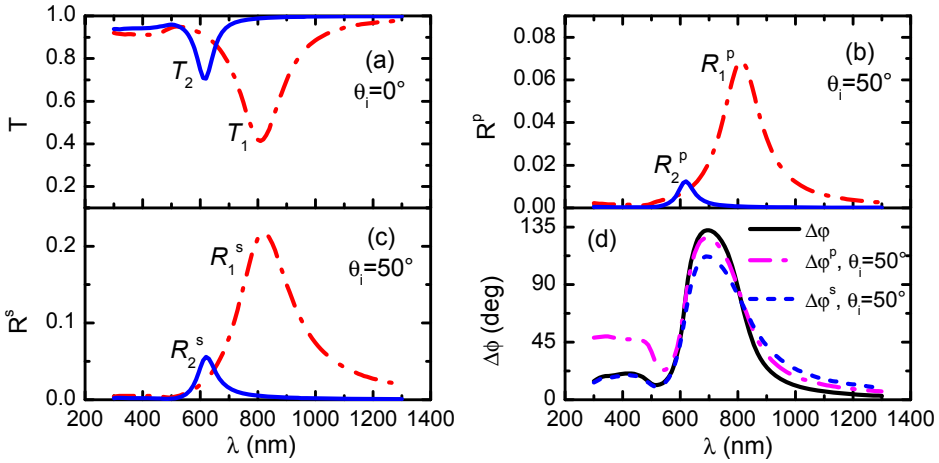

Fig. 4. Island film theory calculated spectra for individual free-standing nanosdisks layers shown in Fig. 3(b): (a) normal incidence transmittance, (b) p-polarized and s-polarized (c) reflectance at angle of incidence 50°. (d) Spectral dependence of phase differences between the in-plane polarizabilities of Fig. 2 ($\Delta\varphi$), reflection coefficients for p- ($\Delta\varphi^{\mathrm{p}} = \varphi_1^{\mathrm{p}}$-$\varphi_2^{\mathrm{p}}$) and s-polarized ($\Delta\varphi^{\mathrm{s}} = \varphi_1^{\mathrm{s}}$-$\varphi_2^{\mathrm{s}}$) light at 50° angle of incidence. Subscripts 1 and 2 refer to the bottom and top nanodisks, respectively.

3.4 Interference effects in free-standing and supported two-island layers

In this section, we first investigate interference effects in the hypothetical system shown in Fig. 3(c) which is comprised by two free-standing gold nanodisks layers, separated by a distance h and immersed in an ambient of refractive index n_a. The scattering matrix of this system is $\mathbf{S} = \mathbf{I}_{f2}\mathbf{L}_h\mathbf{I}_{f1}$ where the top and bottom nanodisks layers are represented with interface matrices $\mathbf{I}_{f2}$ and $\mathbf{I}_{f1}$ of the type given in Eq. (10) and $\mathbf{L}_h$ is the standard layer matrix $\mathbf{L}_h = \mathrm{diag}\left[\exp\left(-i\phi\right), \exp\left(+i\phi\right)\right]$ with $\phi = khn_a\cos\theta_i$ and $h = s + c_1 + c_2$. This phase shift is introduced by the electromagnetic waves traveling back and forth in the region bounded by

#178926 - $15.00 USD Received 1 Nov 2012; revised 28 Nov 2012; accepted 28 Nov 2012; published 20 Dec 2012

the two interfaces of the nanosandwich structure as represented in Fig. 3(d). Thus, the reflectance of this system for p- and s-polarization $R^{p,s} = \left|S_{21}^{p,s} / S_{11}^{p,s}\right|^2$ is given by,

$$R^{p,s} = \frac{R_2^{p,s} + R_1^{p,s}\left|t_2^{(p,s)2} - r_2^{(p,s)2}\right|^2 + 2\sqrt{R_1^{p,s}R_2^{p,s}}\left|t_2^{(p,s)2} - r_2^{(p,s)2}\right|\cos\Phi^{p,s}}{1 + R_1^{p,s}R_2^{p,s} - 2\sqrt{R_1^{p,s}R_2^{p,s}}\cos\left(\varphi_1^{p,s} + \varphi_2^{p,s} + 2\phi\right)}, \quad (14)$$

where $\Phi^{p,s} = \varphi_1^{p,s} - \varphi_2^{p,s} + 2\phi + \delta^{p,s}$ and $\delta^{p,s}$ is the phase of $t_2^{(p,s)2} - r_2^{(p,s)2}$. The cosine term in the numerator of Eq. (14) produces interference effects. The transmittance is obtained from $T_d^{p,s} = \left|1/S_{11}^{p,s}\right|^2 = T_1^{p,s}T_2^{p,s}/D^{p,s}$ where $D^{p,s}$ is the denominator in Eq. (14) and no interference effects are expected in transmission spectra.

Figure 5(a) shows the calculated spectrum at normal incidence of the two interfaces system and clearly $T_d \approx T_1T_2$. However, in Figs. 5(b) and 5(c) the reflectance spectra R^p and R^s calculated with Eq. (14) for p- and s-polarization, respectively, exhibit strong destructive interference at λ = 660 nm coincident with what is experimentally observed in Fig. 1(c). In the case of p-polarization the reflectance decreases with increasing angle of incidence from 20 to 70°, as indicated by the arrow in Fig. 5(b), because the contribution of $\alpha_{j,\parallel}$ decreases continuously with increasing angle of incidence. On the contrary, R^s increases and broadens at grazing angles of incidence. The fact that different interference effects arose depending on the observation conditions (reflection or transmission) has previously been reported in other plasmonic systems [16]. The Fano-like interference in Figs. 5(b) and 5(c) results from the coherent addition of electromagnetic waves reflected from the nanodisks layers and determined by the phase $\Phi^{p,s}$ in Eq. (14) whose spectral dependence for p-polarization is shown in Fig. 5(d). Actually, $\delta^{p,s}$ is very small and the interference is dominated by the other terms in $\Phi^{p,s}$. Similar results were obtained for s-polarization (not shown).

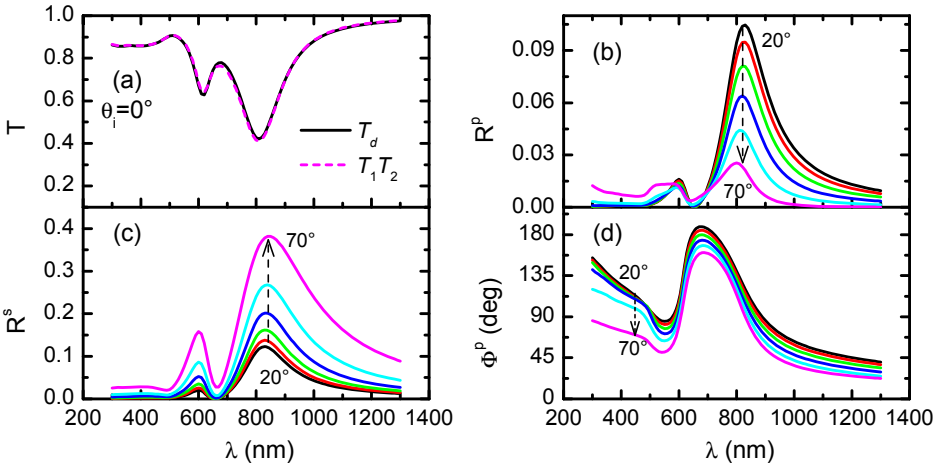

Fig. 5. Island film theory calculated spectra for two free-standing nanosdisks layers shown in Fig. 3(d) immersed in air and separated by 60 nm. (a) Normal incidence transmittance; (b) p-polarized reflectance and (c) s-polarized reflectance at angles of incidence between 20 and 70° (in steps of 10°). (d) Spectral dependence of the phase $\Phi^p = \varphi_1^p - \varphi_2^p + 2\phi + \delta^p$ in Eq. (14) for p-polarization. In (a) also is shown the product T_1T_2 of spectra shown in Fig. 4(a).

The formalism in the last paragraph is readily extended for supported gold nanosandwiches. For this system the scattering matrix is $\mathbf{S} = \mathbf{I}_{f2}\mathbf{L}_h\mathbf{I}_{f1}\mathbf{L}_{a1}\mathbf{I}_{as}$ where $\mathbf{I}_{as}$ is the normal Abelès ambient-substrate interface matrix [33]. Figure 6 shows a comparison between simulated and experimental spectra. As can be observed for R_s in Figs. 6(a) and 6(b) at θ_i = 50° and 70°, respectively, all the features in the experimental spectra are reproduced by the

#178926 - $15.00 USD Received 1 Nov 2012; revised 28 Nov 2012; accepted 28 Nov 2012; published 20 Dec 2012

simulation, including the destructive Fano interference at λ = 660 nm. A close inspection of the R_s spectra in Figs. 6(a) and 6(b) reveals that they are less broad than the calculated spectra shown in Fig. 5(c). This observation indicates that interference effects associated with reflections from the substrate are also present. On the other hand, it can be noticed that the experimental R_p spectra are well described by the model-calculated data, including the inverted line-shape at an angle of incidence of 70°, which is not seen in Fig. 5(c) because it is caused by the presence of the substrate. Furthermore, the model-calculated R_p spectrum in Fig. 6(b) shows weaker constructive interference and the minimum at about λ = 800 nm is slightly blue-shifted. It is clear that modeling the nanodisks as oblate spheroids represents some limitations. In particular, the sharpness of edges and interfaces in the real structure (which obviously have been neglected) strongly modify the screening effects mainly on the out-of-plane components ($\alpha_{j,\perp}$) controlling the p-reflectance and an increasing effect with the angle of incidence is expected.

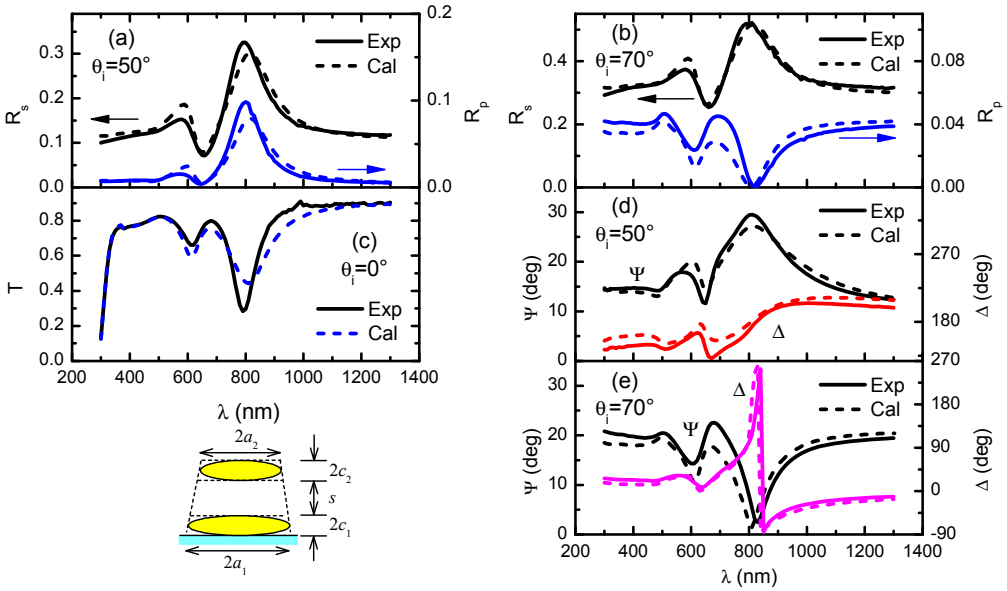

Fig. 6. Experimental and island film theory calculated spectra for nanosandwiches: p- and s-polarized reflectance at angles of incidence (a) 50° and (b) 70°; (c) normal incidence transmittance; ellipsometric spectra at angles of incidence (d) 50° and (e) 70°. The two non-interacting oblate spheroids representing the nanosandwiches are schematically shown at the bottom-left.

Figure 6(c) shows the normal incidence overall transmittance of light exiting from the back side of the substrate calculated according to,

$$T = \left|t_{sa}/S_{11}\right|^2 \exp\left(-\alpha_s d_s\right), \tag{15}$$

where t_{sa} is the transmission coefficient of the substrate-ambient back interface (the reflection from this interface is neglected); α_s and d_s are the absorption coefficient and thickness of the substrate, respectively. Finally, Figs. 6(d) and 6(e) show the experimental and model-calculated ellipsometric spectra for Ψ and Δ which are defined by the complex-valued ratio between the reflection coefficients for light polarized parallel r_p and perpendicular r_s to the plane of incidence [33],

$$r_p/r_s = \tan\Psi \exp\left(i\Delta\right). \tag{16}$$

The importance of reporting ellipsometric data resides on the fact that they represent different illumination and measuring conditions, which are incidence of simultaneous p- and s-polarized waves and measurement of their intensity ratio and phase difference. As shown in

#178926 - $15.00 USD Received 1 Nov 2012; revised 28 Nov 2012; accepted 28 Nov 2012; published 20 Dec 2012

Figs. 6(d) and 6(e) there is a very good agreement between experimental and model-calculated data sets at angles of incidence of 50 and 70°, thus supporting to the reliability of the model employed as well as the use of the nominal structural parameters.

3.5 Homogenization of nanosandwiches layers

The results of the previous sections clearly show that homogenization of the nanosandwich layer is not possible, that is, the internal structure of the sample cannot be neglected. Nevertheless, previously we reported homogenization of supported nanodisks using the effective medium Yamaguchi expressions [30]. Therefore, this approach represents a homogenization alternative to be explored for the layers comprising the nanosandwich. In this case, the sample is represented as a three-layer system on glass which is depicted in the inset of Fig. 7(c). In this system, each layer has uniaxial anisotropy with effective in-plane ($\varepsilon_{j,||}$) and out-of-plane ($\varepsilon_{j,\perp}$) components of the complex dielectric tensor of the Yamaguchi type [28,30],

$$\varepsilon_{j,||} = \varepsilon_a \left[1 + q_j \alpha_{j,||} / V_j \right], \tag{17}$$

and,

$$\varepsilon_{j,\perp} = \varepsilon_a \left[1 - q_j \alpha_{j,\perp} / V_j \right]^{-1}. \tag{18}$$

Here, q_j is the volume fraction occupied by the nanodisks with volume V_j in layer j (= 1,2) and polarizabilities $\alpha_{j,(||,\perp)}$ of Eq. (1) and Fig. 2. Figure 7 shows the in-plane ($\varepsilon_{j,||}$) and out-of-plane ($\varepsilon_{j,\perp}$) components of the effective complex dielectric tensor for the bottom (j = 1) and top (j = 2) nanodisks layers. As expected, $|\varepsilon_{1,||}| > |\varepsilon_{2,||}|$ and $|\varepsilon_{1,\perp}| > |\varepsilon_{2,\perp}|$ because of the same reasons as discussed above in the case of the nanodisks polarizabilities in Fig. 2. For the spacer layer the polarizabilities in Eqs. (17) and (18) were calculated with $\varepsilon_m = \varepsilon_{silica}$ in Eq. (1) and geometric depolarization factors $l_{2,||}$ and $l_{2,\perp} = 1 - 2l_{2,||}$ using the nominal values of the structural parameters. The resulting tensor components are close to unity.

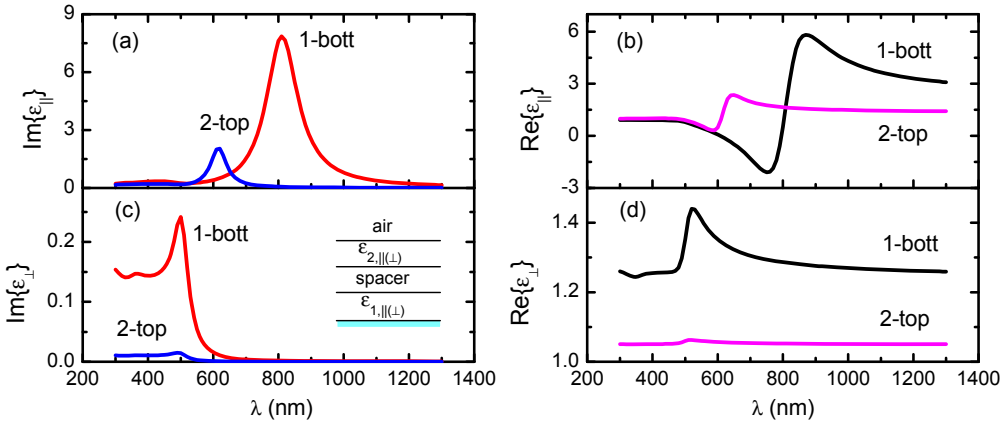

Fig. 7. Effective dielectric function tensor components of gold nanodisks layers: (a)-(b) in-plane $\varepsilon_{||}$ and (c)-(d) out-of-plane $\varepsilon_{\perp}$. The inset in (c) depicts the three homogeneous layers system. The space layer has real-valued dielectric functions components close to unity.

Figure 8 shows the experimental and calculated spectra of R_s, R_p, Ψ, and Δ using the air-three uniaxial layers-glass system and the 4 × 4 matrix Berreman method [33]. The film thicknesses for the layers were the nominal nanodisks thicknesses namely, 20, 40, and 20 nm and the volume fractions q_j were 0.075, 0.064, and 0.037 for layer 1, spacer layer and layer 2, respectively. As can be observed in Figs. 8(a) and 8(b), the calculated data reproduce the

#178926 - $15.00 USD Received 1 Nov 2012; revised 28 Nov 2012; accepted 28 Nov 2012; published 20 Dec 2012

Fano line-shape of the R_s and R_p spectra quite well at the two angles of incidence θ_i = 40 and 70°, respectively. The experimental and simulated spectra of the ellipsometric angles Ψ and Δ at the two angles of incidence are shown in Figs. 8(c) and 8(d), respectively. The homogenized layers model description of the experimental spectra in Fig. 8 is clearly similar to the one based on the island film theory in Fig. 6. In particular, both models give an excellent representation of both plasmon resonances and the experimentally observed Fano interference.

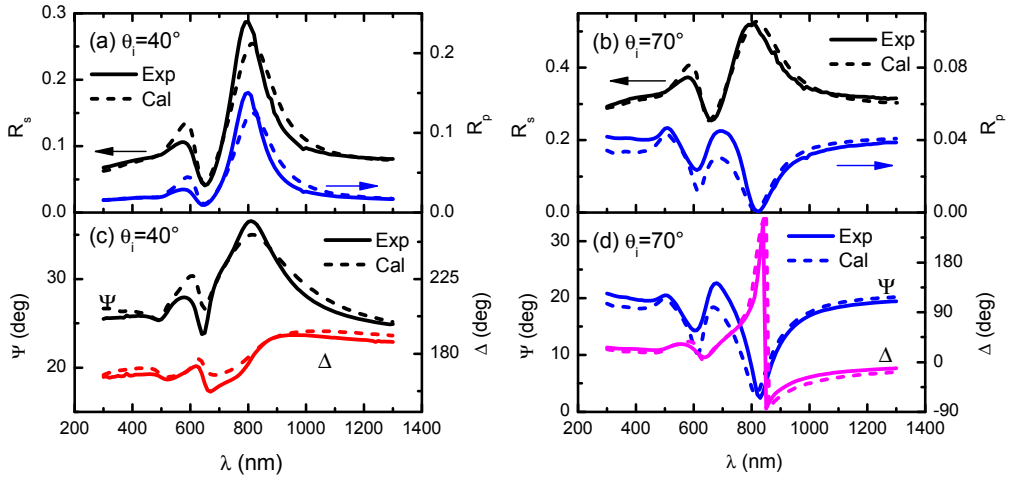

Fig. 8. Experimental and calculated three-effective layers spectra of: p- and s-polarized reflectance at angles of incidence (a) 40° and (b) 70°; ellipsometric spectra of Ψ and Δ at (c) 40° and (d) 70°.

4. Conclusions

We have presented a theoretical analysis of experimental spectra of a layer of gold nanosandwiches comprised of two weakly coupled 20 nm thick gold nanodisks separated by a 40 nm silica spacer. It was found that modified Fresnel coefficients based on an island film theory and the Abelès 2 × 2 scattering matrix formalism accurately describe all experimental features observed, including ellipsometry data and spectral interference effects of the Fano type. The surface susceptibilities required by the island film theory were modeled by approximating the nanodisks as oblate spheroids while taking into account the interaction with the substrate. The asymmetric Fano line-shape observed in the reflectance spectra results from coherent superposition and interference of electromagnetic waves being reflected by the individual nanodisks layers and the substrate. Recently, pronounced Fano interference between localized plasmons and interface reflection was reported for layers of nanodisks made by hole-mask colloidal lithography [18]. However, in that case, the measurements were performed with light incident from the glass side. In particular, the strongest Fano effect was observed for angles close to the critical angle, that is, close to the transition from a spectral reflectance peak, similar to the spectral features discussed here, and a spectral dip observed under total internal reflection. In the present case, the Fano effect is instead dominated by interference between the light emerging from the two nanodisk layers comprising the sandwich structure. The strongest interference is found for wavelengths in between the plasmon resonances of the individual nanodisks, corresponding to out-of-phase oscillations of the decoupled nanodisks plasmons. As an alternative approach, we show that the measured spectra can also be well described through homogenization of the individual layers in the nanosandwiches array using dielectric functions of the Yamaguchi type.

#178926 - $15.00 USD Received 1 Nov 2012; revised 28 Nov 2012; accepted 28 Nov 2012; published 20 Dec 2012

Acknowledgments

AMG acknowledges the support of Conacyt-Mexico and of the "Fondo Sectorial de Investigación para la Educación" grant No. 103385. The Knut and Alice Wallenberg foundation is acknowledged for support to instrumentation. MK and AD acknowledge support from the Swedish Foundation for Strategic Research through the grant RMA08 Functional Electromagnetic Metamaterials.

#178926 - $15.00 USD Received 1 Nov 2012; revised 28 Nov 2012; accepted 28 Nov 2012; published 20 Dec 2012